

Robust Geospatial Coordination of Multi-Agent Communications Networks Under Attrition

Jonathan S. Kent^{1,2,*}, Eliana Stefani³, Brian Plancher^{4,5}

Abstract—Fast, efficient, robust communication during wildfire and other emergency responses is critical. One way to achieve this is by coordinating swarms of autonomous aerial vehicles carrying communications equipment to form an ad-hoc network connecting emergency response personnel to both each other and central command. However, operating in such extreme environments may lead to individual networking agents being damaged or rendered inoperable, which could bring down the network and interrupt communications. To overcome this challenge and enable multi-agent UAV networking in difficult environments, this paper introduces and formalizes the problem of Robust Task Networking Under Attrition (RTNUA), which extends connectivity maintenance in multi-robot systems to explicitly address proactive redundancy and attrition recovery. We introduce Physics-Informed Robust Employment of Multi-Agent Networks (ΦIREMAN), a topological algorithm leveraging physics-inspired potential fields to solve this problem. Through simulation across 25 problem configurations, ΦIREMAN consistently outperforms the DCCRS baseline, and on large-scale problems with up to 100 tasks and 500 drones, maintains > 99.9% task uptime despite substantial attrition, demonstrating both effectiveness and scalability.

Index Terms—Multi-Robot Systems; Distributed Robot Systems; Aerial Systems: Applications

I. INTRODUCTION

Consider a scenario involving the fighting of a forest or city fire, where emergency responders are distributed across multiple hotspots, each requiring constant communication with central command for effective coordination. The problem faced by these responders is not localized to a single point, but may be understood as a collection of tasks each requiring reliable communication (e.g., various outbreaks of flame, possibly moving over time). In such scenarios, communication to all agents at all task areas is essential to mission success, but it may be hampered by absent or destroyed cell infrastructure, or otherwise incur Size, Weight, and Power (SWaP) costs associated with satellite communications equipment [1]–[3]. One potential solution would be to deploy a swarm of networking drones to enable communication; each drone can move spatially, and when within range, communicate with other drones, the operator, and agents localized to each task. If the drones are spatially organized correctly, they will produce an

ad-hoc network that allows agents at each task to communicate with their operator as well as with each other.

However, due to the extreme environment, these network drones may undergo attrition, possibly disabled by heat, smoke, or bad actors [4]. When a drone is attrited in this way, other drones must re-position themselves to re-establish lines of communication, but this still results in temporary disruption to the network. A robust system should therefore have the property that the drone network possesses enough slack and redundancy to ensure that limited drone attrition will not result in a disruption of connectivity to each task.

Similar challenges arise in disaster response [5], [6], search-and-rescue operations [4], [7], and tactical battlefield engagements [8], [9], where maintaining reliable communication networks is critical despite harsh conditions that may damage or destroy networking assets. The common thread across these scenarios is the need for a robust, self-healing network that can maintain connectivity even as individual nodes fail.

Related problems in multi-robot systems have explored task allocation [10]–[16], topology generation and maintenance [17]–[21], spatial coordination [19]–[23], and recovery from failures [24]–[28]. However, much of these efforts do not consider the combined implications of these challenges.

This paper makes three primary contributions. First, we formalize the Robust Task Networking Under Attrition (RTNUA) problem combining task allocation, topology generation and maintenance, and attrition anticipation and recovery with quantitative uptime metrics. Second, we introduce the ΦIREMAN algorithm achieving consistently higher task uptime than purely reactive approaches by proactively creating redundant network geometries via physics-inspired potential fields. Third, we provide comprehensive evaluation across 25 problem size and attrition rate configurations, demonstrating consistent improvements over the DCCRS baseline [29].

II. RELATED WORK

Related problems in multi-robot systems have explored task allocation, topology generation and maintenance, spatial coordination, and recovery from failures. However, as noted above, much of this effort does not consider the combined implications of these challenges. We organize the discussion thematically to clarify how existing work addresses individual aspects, while the RTNUA problem requires their integration.

Multi-Robot Task Allocation. Extensive work addresses multi-robot task allocation (MRTA) [10]–[16]. These approaches focus on assigning agents to tasks but do not address

¹ Advanced Technology Center, Lockheed Martin Space;

² Fu Foundation School of Engineering and Applied Science, Columbia University;

³ Lockheed Martin AI Center, Lockheed Martin Corporation;

⁴ Barnard College, Columbia University;

⁵ Dartmouth College.

*Correspondence to: jonathan.s.kent@lmco.com.

Authors would like to thank Columbia’s Junfeng Yang, CMU’s Katia Sycara and Wennie Tabib, UIUC’s Indranil Gupta and Darci Peoples, and Georgia Tech’s Hazel B. Sparks.

Prior Work	Task Allocation	Topology Generation	Topology Maintenance	Spatial Coordination	Attrition Anticipation	Attrition Recovery
[2], [18]	✓	✓	✓	✓		✓
[10], [30]	✓				✓	
[19]			✓	✓	✓	
[20], [21]	✓		✓	✓		
[22], [23]			✓	✓		
[24], [31], [32]	✓					✓
[25]	✓			✓		
[26]		✓	✓	✓		✓
[27]	✓		✓		✓	
[28]	✓				✓	✓
[29] (DCCRS)	✓	✓	✓	✓	✓	✓
Ours	✓	✓	✓	✓	✓	✓

Table I: Feature sets and areas of concern for related work. Most works are not able to jointly handle task allocation and the generation and maintenance of network topologies in a geospatial setting, while anticipating and recovering from attrition. In later sections we demonstrate how our approach outperforms the DCCRS [29] baseline. Works are grouped according to features and concerns only, not on any basis of their operation.

the critical networking behavior among agents, specifically determining geometric locations to ensure a connected network. For example, work such as [10], [30] optimizes assignments but treats communication as a constraint rather than a spatial coordination problem for co-design.

Network Topology Generation and Maintenance. Research on topology generation and maintenance [17]–[21] ensures connectivity but typically assumes pre-allocated agents. Work on robust k -connectivity in swarm networks, such as [19], assumes that each agent is already assigned to a given task and that the network maintains k -connectivity throughout. Crucially, these approaches provide no method for recovering connectivity if it is lost due to attrition. Similarly, while [20] develops geometrically connected spanning trees among pre-tasked agents, it does not consider robustness or goal states. The algorithm in [21] jointly solves both the MRTA problem and the networking problem geometrically but again does not respond to or anticipate attrition.

Spatial Coordination. Approaches to spatial coordination [22], [23] achieve local interactions among robots but focus on collision avoidance or formation control rather than network topology optimization. While these methods demonstrate emergent behaviors from local rules, they do not explicitly optimize for communication network properties or task connectivity.

Robustness to Failures. Research focused on attrition within agent swarms typically centers on reacting to attrition once it occurs, rather than enabling robustness prior to attrition. Works such as [31]–[33] primarily address task assignments rather than networking. While [26] considers failures of particular resources on networked agents, it does not account for the complete loss of agents nor pre-configure the network to prevent temporary outages due to such attrition. The problem in [27] adapts to attrition of surveillance agents by modifying remaining agents’ routes but does not plan ahead for attrition or address networking constraints. Although [30] plans routes to minimize capital loss due to attrition, it focuses on reducing

attrition risk rather than maintaining network effectiveness despite assumed attrition. In [28], agent attrition results from direct combat, with fundamentally different dynamics.

Positioning Our Contribution. As shown in Table I, of these related works, only [29] treats every desired component of the RTNUA problem. The algorithm presented, denoted DCCRS in the absence of a name given in the manuscript, uses potential fields from attraction, repulsion, and velocity matching of neighbors, as well as specific modifications relating to density and distance-to-leader to maintain network coherence. However, DCCRS was designed only to retain network coherence under attrition, and while it implicitly has elements of recovery mechanisms, this was not a point of explicit design for DCCRS, nor was it treated in their experiments, which end as soon as decoherence occurs for the first time. Our approach considers all of these factors, and extends physics-based swarm modeling [34]–[37] to organize drones into robust network geometries, and is demonstrated with metrics that capture both network maintenance and recovery capabilities.

III. ROBUST TASK NETWORKING UNDER ATTRITION

To enable precise algorithm development and evaluation, we formalize the RTNUA problem mathematically. The formalization captures three key requirements: drones must maintain network connectivity through spatial coordination, tasks require continuous connection to a base station, and random attrition degrades the network over time. We introduce two complementary metrics, $TU1$ measuring overall task uptime and $TU2$ discounting the exploration phase, to evaluate algorithms comprehensively rather than simply measuring time-to-first-failure as in prior work.

A. Problem Formulation

We now formalize the Robust Task Networking Under Attrition (RTNUA) problem. A set of n drones $\mathcal{D} = \{D_1, D_2 \dots D_n\}$ is distributed spatially about \mathbb{R}^2 , with a controller existing at

a base station B located at the origin, with a communication radius R . Each drone D_i is represented at time t by the tuple $D_i(t) = (\mathbf{x}_i(t), \lambda_i, r_i, v_i, e_i(t), a_i(t))$, where:

- $\mathbf{x}_i(t) \in \mathbb{R}^2$ gives its position relative to the base station as a vector in \mathbb{R}^2
- $\lambda_i \in \mathbb{R}_{>0}$ gives its attritional half-life
- $r_i \in \mathbb{R}_{>0}$ is its maximum radius of two-way communication
- $v_i \in \mathbb{R}_{>0}$ is its maximum speed
- $e_i(t) \in \{\text{TRUE}, \text{FALSE}\}$ gives its current state of attrition, FALSE meaning it is alive and unattrited
- $a_i(t) \in \{\text{TRUE}, \text{FALSE}\}$ gives its current activation state

Two drones D_i, D_j can only communicate if $|\mathbf{x}_i - \mathbf{x}_j| \leq \min(r_i, r_j)$. For a given duration δt , each drone has the speed restriction $|\mathbf{x}_i(t + \delta t) - \mathbf{x}_i(t)| < v_i \delta t$. Drones start unattrited with $e_i(0) = \text{FALSE}$, and for duration δt , undergo attrition with probability $p_i(\delta t) = 1 - 0.5^{\delta t / \lambda_i}$, such that $e_i(t + \delta t) = e_i(t) \vee \text{Bern}(p_i(\delta t))$. An attrited drone cannot be restored. This model of attrition was selected for computational simplicity, and more complex or geographically localized attrition can be treated in future work.

A drone is considered active if it is both unattrited and network-connected (either directly or indirectly):

$$\begin{aligned} a_i^B(t) &= |\mathbf{x}_i(t)| \leq \min(R, r_i) \\ a_i^d(t) &= (\exists D_j \in \mathcal{D} \mid a_j(t) \wedge |\mathbf{x}_i(t) - \mathbf{x}_j(t)| \leq \min(r_i, r_j)) \\ a_i(t) &= \neg e_i(t) \wedge (a_i^B(t) \vee a_i^d(t)) \end{aligned} \quad (1)$$

The system includes m tasks $\mathcal{T} = \{T_1, T_2, \dots, T_m\}$. Practically speaking, each task would be an agent or set of agents requiring network connectivity, e.g. a group of firefighters, a member of the infantry, an unmanned ground vehicle, etc. Each task is represented as $T_i(t) = (\mathbf{y}_i(t), A_i(t))$, with position $\mathbf{y}_i(t) \in \mathbb{R}^2$ and connection state $A_i(t) \in \{\text{TRUE}, \text{FALSE}\}$. A task is connected if at least one active drone is within range:

$$A_i(t) = \exists D_j \in \mathcal{D} \mid a_j(t) \wedge |\mathbf{y}_i(t) - \mathbf{x}_j(t)| < r_j \quad (2)$$

Denoting these as "tasks" is intended to stay in-line with [19], [20], and [21], and are considered equivalent to the "leader drones" from [29].

A controller \mathcal{C} receives the set of networked drones $\mathcal{D}'(t) = \{D_i \in \mathcal{D} \mid a_i(t)\}$ and all tasks \mathcal{T} , providing motion instructions $\delta \mathbf{X}(t) = \{\delta \mathbf{x}_i(t)\}$ bounded by $|\delta \mathbf{x}_i(t)| \leq v_i$. For networked drones, $\mathbf{x}_i(t + \delta t) = \mathbf{x}_i(t) + \delta t \delta \mathbf{x}_i(t)$. For experimental purposes, we include a default behavior wherein unattrited but disconnected drones move directly toward the base station at constant speed until reconnected or destroyed, again leaving further development in this area to future work.

B. Objective Functions for Solution Benchmarking

The objective functions for RTNUA are closely related to established metrics from multi-robot systems and network

algorithm literature. Network uptime ratios, expressed as $U = (T_{\text{operational}} / \tau)$, have been extensively used to quantify system reliability in surveillance and monitoring applications. Similarly, temporal connectivity measures such as connectivity persistence $CP = (1/\tau) \int_0^\tau a(t) dt$, where $a(t)$ indicates connectivity at time t , provide mathematical frameworks for evaluating time-varying network performance [38], [39].

Building on these foundations, we define the primary objective to maximize expected task uptime:

$$TU1 = \mathbb{E}_{\text{scenario}} \left[\int_{t=0}^\tau \frac{1}{m} \sum_{T_i \in \mathcal{T}} A_i(t) dt \right] \quad (3)$$

This formulation provides an appropriate communication uptime metric for the multi-task setting, where the proportion of time communication links remain active is generalized to the average connectivity across all tasks, where a task is connected if it is within range of an active networked drone. The metric aligns with coverage quality metrics in wireless sensor networks that employ temporal coverage quality $\int_0^\tau C(t) dt$ where $C(t)$ represents the coverage function [40], [41].

A secondary objective accounts for the speed of exploration by only considering tasks after initial connection:

$$TU2 = \mathbb{E}_{\text{scenario}} \left[\int_{t=0}^\tau \frac{\sum_{T_i \in \mathcal{T}} A_i(t) dt}{\sum_{T_i \in \mathcal{T}} \exists t' \in [0, t] \mid A_i(t')} \right] \quad (4)$$

This metric is related to the monitoring coverage ratios used in persistent surveillance literature, particularly in connectivity-constrained multi-robot persistent surveillance frameworks where robots must visit sensing locations periodically while maintaining network connectivity [42]. The normalization by discovered tasks reflects similar approaches in multi-UAV cooperative systems where performance metrics account for the proportion of targets under surveillance throughout the mission [43], [44]. By providing this second metric, we can consider an algorithm's ability to maintain network uptime both in the context of and discounting its speed of exploration.

The metric used in [29], introducing DCCRS, was only the length of time until network decoherence first occurs. While this is meaningful for the problem of faultless network maintenance, it does not capture any information about the severity of failures, the magnitudes of their effects on users of the network, or how well the system might recover from failures afterwards. Our formulations are intended to capture these and other challenges of maintaining robust network connectivity despite ongoing attrition, while allowing for practical constraints like limited communication ranges and drone velocities.

IV. ΦIREMAN ALGORITHM

To provide a state-of-the-art solution to the RTNUA problem, we developed the Physics-Informed Robust Employment of Multi-Agent Networks, or ΦIREMAN, algorithm as a computationally efficient baseline that leverages physics-inspired local interactions to achieve emergent robustness without

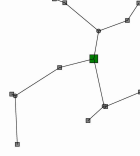


Figure 1: Semi-Steiner task tree example with $c_b = 0.3$, balancing total edge length ($l_{\Sigma e} = 19.86$) against sum of distances to base station ($l_{\Sigma b} = 39.53$). Steiner nodes (circles) enable more efficient network topologies.

requiring complex learning algorithms or extensive inter-agent communication. Φ IREMAN is based upon leveraging the topological properties of efficient sphere packings in 2 dimensions, insofar as they spontaneously generate hexagonal meshes in low energy configurations. By combining a potential field that has been designed to encourage desired network geometries with synthetic attractive and repulsive forces akin to those observed in polar fluids at the molecular level, we can engineer an energy manifold for which low energy states represent the network occupying a designed geometry and exhibiting a hexagonal mesh pattern. By driving the combined network system towards those low energy states, we theorize and then observe regenerating network contiguity, robustness to attrition, exploration, and efficient spatial coverage all manifesting as emergent behaviors.

A. The Computational Difficulties of Solving RTNUA

Calculating the expected uptime of tasks under the RTNUA formulation presents significant computational challenges due to the fundamental intractability of percolation theory in continuum systems. Unlike discrete lattice percolation with some exact solutions for specific cases [45], continuum percolation systems lack general analytical solutions [46], [47] and require computationally intensive Monte Carlo simulations [48], making direct optimization approaches prohibitively expensive for real-time use. While decentralized multi-agent reinforcement learning (MARL) offers a general approach to distributed decision-making, robust MARL systems require extensive offline training [49], significant inter-agent communication overhead scaling quadratically with agent count [50], and substantial computational resources unsuitable for resource-constrained edge devices [51]. These factors motivate the development of Φ IREMAN as a computationally efficient baseline that leverages physics-inspired local interactions to achieve emergent robustness without requiring complex learning algorithms or extensive inter-agent communication, further differentiated from DCCRS [29] by removing velocity matching and leader following behaviors in favor of directly approximating a Steiner tree.

B. Task-Space Potential Field

We develop the geometry of the task space potential field by first constructing a graph that connects tasks to the base station. The potential at any location is then given by its distance to

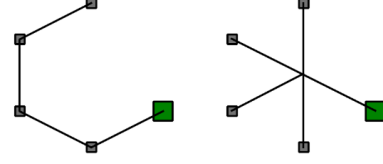


Figure 2: Left; hypothetical task tree graph using only sum of distances, right; task tree graph including sum of distances to base station.

the nearest point on this graph. While a minimal spanning tree would minimize total edge length, it can produce geometries that are counter to robustness, e.g. in the event that tasks form a horseshoe-shape with the base station located at one end, the minimal spanning tree would produce a geometry that would result in disconnection of the opposite end given an individual failure at any point along the curve, see Figure 2.

Instead, we jointly minimize the total graph length $l_{\Sigma e}$ and the sum of path distances from tasks to base station $l_{\Sigma b}$. The latter objective encourages more direct routes, reducing potential single points of failure. Additionally, since this is a geometric rather than purely topological problem, we greedily approximate a Steiner tree, inserting auxiliary Steiner nodes to reduce overall distance costs.

The weighting coefficient c_b controls the trade-off between minimizing edge length and minimizing distances to base station. Higher values of c_b produce more direct routes at the cost of increased total edge length. An example of a semi-Steiner task tree can be found in Figure 1.

C. Swarm Dynamics

Rather than explicitly simulating fluid dynamics with momentum, we use gradient descent on an energy manifold to drive drones toward low-energy configurations. This replicates the desired fluid-like behaviors more efficiently in both computation and motion. The total potential energy for drone D_i is given by:

$$E_i^{\Sigma} = E_i^b + E_i^{\mathcal{M}} + E_i^P \quad (5)$$

where,

$$\begin{aligned} E_i^b &= \mathbf{P} \cdot h^T(\mathbf{x}_i) & E_i^{\mathcal{M}} &= \mathcal{M} \cdot \sum_{D_j \in \mathcal{D} | i \neq j} \frac{-1}{|\mathbf{x}_j - \mathbf{x}_i|} \\ E_i^P &= \frac{P}{2} \cdot \sum_{D_j \in \mathcal{D}'} (q_i + q_j - |\mathbf{x}_i - \mathbf{x}_j|)^2. \end{aligned} \quad (6)$$

In this setup, we use $\mathbf{P} \cdot h^T(\mathbf{x}_i)$ to represent the potential due to the task space potential field geometry, \mathcal{M} to represent the attraction between drones, and P to represent elastic repulsion between drones when closer than $q_i + q_j$. We note that \mathcal{D}' in the P term enumerates drones within repulsion range and q_i is nominally set to $r_i/2$ such that repulsion activates within communication range.

At each timestep, the controller \mathcal{C} performs multiple steps of gradient descent on the total energy $\mathcal{E}(t, \delta \mathbf{X}(t)) =$

$\sum_{D_i \in \mathcal{D}'(t)} E_i^\Sigma$ to generate motion instructions $\delta \mathbf{X}(t)$. Descent terminates when equilibrium is reached, maximum steps are taken, or any instruction would exceed drone speed limits. Motion instructions are then executed, with drones that have undergone attrition ceasing all movement.

D. Network Maintenance

As tasks move, Steiner node locations are continuously recalculated as the Fermat points of their three neighboring nodes. The complete task tree topology is periodically recomputed, with the new topology accepted if $l_\Sigma^{\text{new}} < \nu \cdot l_\Sigma^{\text{curr}}$, where $\nu \in (0, 1]$ is a threshold coefficient and $l_\Sigma = l_{\Sigma e} + c_b \cdot l_{\Sigma b}$.

Reaction to drone attrition requires no further extension. The potential field naturally causes neighboring drones to flow into gaps while maintaining network connectivity. The redundancy inherent in the hexagonal packing means that a small number of losses can be absorbed without disrupting the network.

E. Asynchronicity and Message Passing

To more closely resemble practical deployments, we introduce asynchronicity and message passing. Each drone maintains knowledge of its own position and broadcasts information to neighbors, received in the subsequent timestep. The Φ IREMAN message passing scheme recursively forwards neighbor locations, retaining the most recent timestamp when receiving duplicate reports and discarding information that becomes too outdated or spatially distant, with thresholds determined via grid search. The Semi-Steiner tree is calculated centrally by the base station, which is assumed to have perfect, synchronous knowledge of task locations, and distributed throughout the network via packet forwarding, with updates following the same recency rule. Drones make kinematic decisions using only their local tree copy and locally known neighbor positions without accounting for information age. When the local task tree becomes too outdated, drones assume disconnection and navigate toward the known base station location as a recovery behavior, resuming normal operation upon re-establishing network contact.

V. EXPERIMENTAL EVALUATION

A. Experimental Setup

We evaluate Φ IREMAN using a simulated environment with the following default configurations of both the underlying RTNUA problem and Φ IREMAN algorithm, using parameters determined via a grid search:

- 10 tasks uniformly distributed in $[-5, 5] \times [-5, 5] \subset \mathbb{R}^2$
- Base station at origin $(0, 0)$
- 50 drones initialized in a radius-1 ring about the base station with Gaussian noise ($\sigma = 0.2$)
- Communication radius $r_i = 2$, repulsion radius $q_i = 1$
- Maximum drone speed $v_i = 0.15$, with a probability of attrition per-simulation step of 1%
- Tasks random walk with Gaussian noise ($\sigma = 0.1$)
- Scenario length of 200 timesteps
- Task distance cost $c_b = 1.0$, topology threshold $\nu = 0.99$
- Potential field coefficients: attraction $\mathcal{M} = 0.05$, repulsion $P = 0.3$, task potential $\mathbf{P} = 0.05$

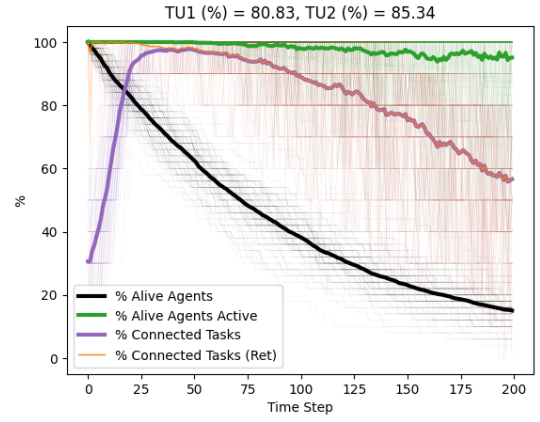


Figure 3: Performance over time of Φ IREMAN under the default configuration. Thick lines give per-timestep averages over 100 simulations. "Alive Agents" shows how many drone agents remain alive; "Alive Agents Active" shows the portion of alive agents which are networked; "Connected Tasks" shows how many tasks are connected; and "Connected Tasks (Ret)" shows how many of the previously connected tasks are currently connected. Once all tasks are connected for the first time, these last two overlap. The integral of the former is $TU1$, and the integral of the latter is $TU2$.

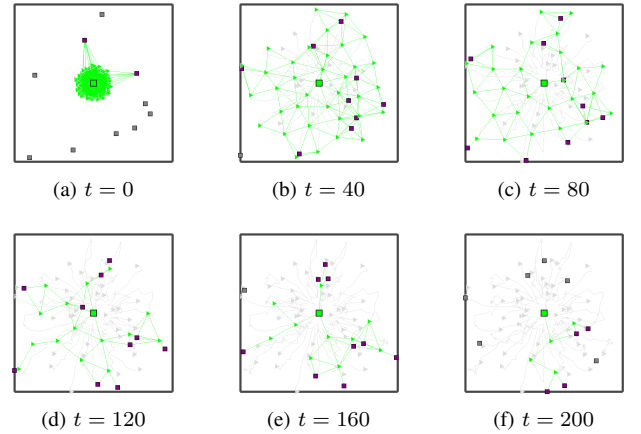


Figure 4: Evolution of drone network under default configurations at $t = 0, 40, 80, 120, 160, 200$ timesteps. Alive drones (green triangles when active, red when disconnected) maintain connectivity between tasks (purple squares when networked, gray when disconnected) and base station (green square) despite ongoing attrition (gray triangles). The gray square is the field border. Green lines are network connections.

B. Baseline Performance

Under default conditions, Φ IREMAN achieves task uptimes of $TU1 = 80.83\%$ and $TU2 = 85.34\%$. While this may appear modest compared to traditional network uptime metrics, it is achieved under substantial attrition with no hard-coded recovery mechanism. To gain intuition for the spatial problem being solved, the drone network evolution at $t = 0, 40, 80, 120, 160, 200$ timesteps is shown in Figure 4. We note that this default setting is also a particularly chal-

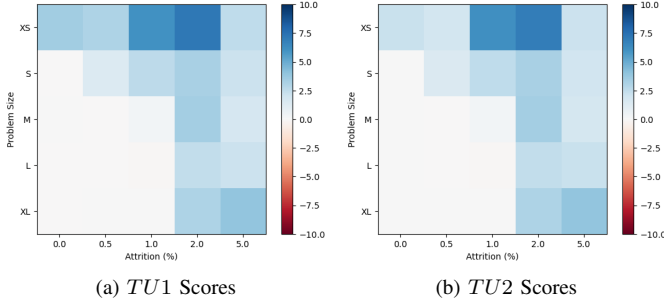


Figure 5: Heatmap of differences between Φ IREMAN and DCCRS $TU1$ and $TU2$ scores on problem configurations. Values shown are the result of subtracting the $TU1$ and $TU2$ scores of DCCRS from those of Φ IREMAN for each configuration. Note that Φ IREMAN generally outperforms DCCRS across all problems and has a maximum performance deficit of only 0.1 percentage points on $TU1$.

lenging one, as on larger problem sizes, with up to 100 tasks, exploration-discounted task uptime $TU2$ exceeds 99.9%, even with substantial attrition. We detail these ablated results, as compared to DCCRS [29], in the following.

C. Comparison Against DCCRS

To explore the relationship between algorithmic performance, problem size, and attrition rate, we provide comparisons between Φ IREMAN and DCCRS [29] over five different problem sizes and five different attrition rates, for a total of 25 configurations. Problem sizes range from extra small, "XS", to extra large, "XL", with values for the number of drones, number of tasks, and field size provided in Table II, as well as per-tick attrition rates of 0%, 0.5%, 1%, 2%, and 5%. For our implementation of DCCRS, hyperparameters with equivalents in Φ IREMAN were carried over exactly, with all other hyperparameters determined via grid search for the default small, 1% attrition rate setting, and held constant over other configurations. We simulated 100 different scenarios for each configuration, with identical scenarios run against both Φ IREMAN and DCCRS by means of seeded random number generation, for a total of 5,000 simulations. Results are shown graphically as heatmaps in Figure 5 and in Table III.

These results show strong and consistent outperformance by Φ IREMAN over DCCRS, with a maximum improvement of over 7 percentage points of $TU1$ in the extra small problem size with an attrition rate of 2%, and a maximum performance deficit of only 0.1 percentage points of $TU1$ in the large problem size with an attrition rate of 1%. These results demonstrate that the Φ IREMAN algorithm performs better than the state-of-the-art.

D. Ablation Studies

We additionally conduct ablation studies to analyze the impact of each algorithm and simulation component, with results presented in Table IV. All ablations are done in the context of the default configurations presented in Section V-B. These ablation studies suggest that Φ IREMAN performs robustly

Problem Size	Drones	Tasks	Field
XS	20	5	$[-2, 2] \times [-2, 2]$
S	50	10	$[-5, 5] \times [-5, 5]$
M	100	20	$[-10, 10] \times [-10, 10]$
L	200	50	$[-20, 20] \times [-20, 20]$
XL	500	100	$[-50, 50] \times [-50, 50]$

Table II: Problem sizes for comparison studies.

Configuration		Φ IREMAN		DCCRS	
Size	Attrition (%)	TU1	TU2	TU1	TU2
XS	0.0	92.79	98.69	89.32	96.46
	0.5	79.73	86.97	76.66	85.11
	1.0	61.63	70.51	55.58	64.37
	2.0	38.96	48.60	31.78	41.70
	5.0	21.54	32.64	19.00	30.48
S	0.0	95.62	99.95	95.66	99.91
	0.5	93.86	98.22	92.47	96.78
	1.0	80.83	85.34	78.21	82.78
	2.0	52.39	57.59	49.12	54.32
	5.0	25.57	32.93	23.39	31.03
M	0.0	95.96	99.98	95.95	99.97
	0.5	95.74	99.80	95.78	99.83
	1.0	90.96	95.05	90.66	94.74
	2.0	64.62	68.78	61.25	65.34
	5.0	30.33	35.43	28.62	33.70
L	0.0	96.12	99.97	96.13	99.97
	0.5	96.09	99.97	96.10	99.97
	1.0	95.41	99.26	95.51	99.37
	2.0	75.86	79.75	73.43	77.31
	5.0	36.15	40.27	34.02	38.06
XL	0.0	96.21	99.97	96.22	99.97
	0.5	96.22	99.97	96.21	99.97
	1.0	96.20	99.97	96.19	99.97
	2.0	88.63	92.41	85.56	89.33
	5.0	43.79	47.60	39.82	43.63

Table III: $TU1$ and $TU2$ percentage scores for both Φ IREMAN and DCCRS in a variety of problem configurations. For a given problem configuration, treating $TU1$ and $TU2$ scores independently, where the difference between the performances of each algorithm is greater than 1, the better of the two results is presented in bold, otherwise in default text. Note that Φ IREMAN generally outperforms DCCRS across all problems and has a maximum performance deficit of only 0.1 percentage points on $TU1$.

across problem parameters, and that problem size and attrition rate have dominating effects on performance, as expected.

1) *Task Graph Components*: Removing the task-space potential field entirely ($P = 0$) reduces performance to $TU1 = 75.76\%$, $TU2 = 80.79\%$. While drones form efficient hexagonal patterns with near-perfect inter-drone connectivity, task uptime suffers from lack of guidance toward task positions.

A similar yet slightly worse degradation to $TU1 = 75.21\%$, $TU2 = 80.16\%$ occurs when the edges of the Semi-Steiner tree are removed from the task-space potential field, as drones tend to form clusters around tasks and do not receive stimulus to

form a network between them.

2) *Environmental Factors*: We also examine how various environmental factors affect performance.

Decreasing the drone speed to $v_i = 0.1$ reduces $TU1$ to 78.45% while increasing the speed $v_i = 0.2$ increases $TU1$ to 82.06%, while $TU2$ is largely unchanged from the default in either instance, indicating that speed changes of this magnitude under these conditions primarily effects exploration.

Changing the standard deviation of the random walks of the tasks to $\sigma = 0$, rendering the tasks immobile, actually slightly decreases scores to $TU1 = 80.37\%$ and $TU2 = 85.10\%$, while doubling task walk speed to $\sigma = 0.2$ reduces scores to $TU1 = 80.18\%$ and $TU2 = 84.48\%$. The decrease with immobile tasks occurs because task motion provides natural exploration stimulus, causing drones to adjust positions and discover configuration improvements. With static tasks, drones converge to local energy minima that may not be globally optimal. This suggests future work should incorporate explicit exploration mechanisms for static task scenarios. The decrease with faster task motion demonstrates an increase in problem difficulty as expected.

VI. CONCLUSION AND FUTURE WORK

This paper introduces and formalizes the Robust Task Networking Under Attrition (RTNUA) problem and presents Φ IREMAN (Physics-Informed Robust Employment of Multi-Agent Networks), which achieves robust networking through physics-inspired fluid dynamics modeling to produce emergent behaviors that both anticipate and respond to attrition. Our experimental results demonstrate that Φ IREMAN successfully produces redundant network topologies that maintain connectivity despite ongoing attrition, significantly outperforming DCCRS [29] and establishing a new state-of-the-art for the problem. Problem size and attrition rate emerge as primary constraints on achievable task uptime, with the task-tree potential field geometry proving essential for guiding drones toward effective network configurations.

Several promising directions remain for future work. To focus on formalizing RTNUA and establishing Φ IREMAN's theoretical foundation, we restrict analysis to 2D and uniformly distributed, randomly walking tasks to provide general results without application-specific assumptions. Future work may extend Φ IREMAN to 3D or incorporate task motion prediction for increased deployed performance. Constraining drones within convex polyhedra fitted to task locations could improve efficiency, as drones positioned outside such regions cannot contribute to network redundancy more effectively than those inside. Adaptive parameter tuning mechanisms could balance competing objectives as network conditions evolve. Formal characterization of the relationship between environmental constraints and optimal algorithm parameters would enhance understanding. Future work could also explore large-scale multi-agent reinforcement learning approaches, which more directly optimize swarm performance against uptime [52]–[54]. Finally, hardware demonstrations in field scenarios, paired with

	Configuration	TU1 (%)	TU2 (%)
	Default	80.83	85.34
Task Graph	$\mathbf{p} = 0$	75.76	80.79
	Nodes only	75.21	80.16
Environmental Factors	$v_i = 0.1$	78.45	85.30
	$v_i = 0.2$	82.06	85.64
	$\sigma = 0$	80.37	85.10
	$\sigma = 0.2$	80.18	84.48

Table IV: Ablation study of algorithm components and environmental parameters on task uptime scores. Scores greater than 1 above the default configuration are shown in bold, scores less than 1 below the default configuration are italicized, and scores within ± 1 of the default are shown in default text.

improved underlying local control [55], [56], would validate the algorithm's distributed nature and reliance on local interactions.

REFERENCES

- [1] M. S. Couceiro, D. Portugal, J. F. Ferreira, and R. P. Rocha, "Semfire: Towards a new generation of forestry maintenance multi-robot systems," in *2019 IEEE/SICE International Symposium on System Integration (SII)*, 2019, pp. 270–276.
- [2] J. Hu, H. Niu, J. Carrasco, B. Lennox, and F. Arvin, "Fault-tolerant cooperative navigation of networked uav swarms for forest fire monitoring," *Aerospace Science and Technology*, vol. 123, p. 107494, 2022.
- [3] R. D. Arnold, H. Yamaguchi, and T. Tanaka, "Search and rescue with autonomous flying robots through behavior-based cooperative intelligence," *Journal of International Humanitarian Action*, vol. 3, no. 1, pp. 1–18, 2018.
- [4] F. Maresca, A. Romero, C. Delgado, V. Sciancalepore, J. Paradells, and X. Costa-Pérez, "React: Multi robot energy-aware orchestrator for indoor search and rescue critical tasks," 2025. [Online]. Available: <https://arxiv.org/abs/2503.05904>
- [5] J. P. Queralta, J. Taipalmaa, B. Can Pullinen, V. K. Sarker, T. Nguyen Gia, H. Tenhunen, M. Gabbouj, J. Raitoharju, and T. Westerlund, "Collaborative multi-robot search and rescue: Planning, coordination, perception, and active vision," *IEEE Access*, vol. 8, pp. 191 617–191 643, 2020.
- [6] Z. Ning, Y. Yang, X. Wang, Q. Song, L. Guo, and A. Jamalipour, "Multi-agent deep reinforcement learning based uav trajectory optimization for differentiated services," *IEEE Transactions on Mobile Computing*, vol. 23, no. 5, p. 5818–5834, May 2024. [Online]. Available: <https://doi.org/10.1109/TMC.2023.3312276>
- [7] A. Agrawal, S. J. Abraham, B. Burger, C. Christine, L. Fraser, J. M. Hoeksema, S. Hwang, E. Travník, S. Kumar, W. Scheirer, J. Cleland-Huang, M. Vierhauser, R. Bauer, and S. Cox, "The next generation of human-drone partnerships: Co-designing an emergency response system," in *Proceedings of the 2020 CHI Conference on Human Factors in Computing Systems*, ser. CHI '20. New York, NY, USA: Association for Computing Machinery, 2020, p. 1–13. [Online]. Available: <https://doi.org/10.1145/3313831.3376825>
- [8] R. Yan and A. Julius, "Distributed consensus-based online monitoring of robot swarms with temporal logic specifications," *IEEE Robotics and Automation Letters*, vol. 7, no. 4, p. 9413–9420, Oct. 2022. [Online]. Available: <http://dx.doi.org/10.1109/LRA.2022.3191236>
- [9] R. K. Ramachandran, P. Pierpaoli, M. Egerstedt, and G. S. Sukhatme, "Resilient monitoring in heterogeneous multi-robot systems through network reconfiguration," *IEEE Transactions on Robotics*, vol. 38, no. 1, pp. 126–138, 2022.
- [10] O. Shorinwa, R. N. Haksar, P. Washington, and M. Schwager, "Distributed multirobot task assignment via consensus admm," *IEEE Transactions on Robotics*, vol. 39, no. 3, pp. 1781–1800, 2023.
- [11] M. Braquet and E. Bakolas, "Greedy decentralized auction-based task allocation for multi-agent systems," 2021. [Online]. Available: <https://arxiv.org/abs/2107.00144>
- [12] A. Prorok, M. A. Hsieh, and V. Kumar, "Fast redistribution of a swarm of heterogeneous robots," *EAI Endorsed Transactions on Scalable Information Systems*, vol. 3, no. 10, pp. 249–255, 2016.

- [13] J. Liu and R. K. Williams, "Submodular optimization for coupled task allocation and intermittent deployment problems," *IEEE Robotics and Automation Letters*, vol. 4, no. 4, pp. 3169–3176, 2019.
- [14] B. P. Gerkey and M. J. Mataric, "A formal analysis and taxonomy of task allocation in multi-robot systems," *The International journal of robotics research*, vol. 23, no. 9, pp. 939–954, 2004.
- [15] G. A. Korsah, A. Stentz, and M. B. Dias, "A comprehensive taxonomy for multi-robot task allocation," *The International Journal of Robotics Research*, vol. 32, no. 12, pp. 1495–1512, 2013.
- [16] R. M. Zlot, "An auction-based approach to complex task allocation for multirobot teams," Ph.D. dissertation, Carnegie Mellon University, The Robotics Institute, 2006.
- [17] E. S. Lee, L. Zhou, A. Ribeiro, and V. Kumar, "Graph neural networks for decentralized multi-agent perimeter defense," *Frontiers in Control Engineering*, vol. 4, Jan. 2023. [Online]. Available: <http://dx.doi.org/10.3389/fcteg.2023.1104745>
- [18] Y. Tian, Y. Chang, F. H. Arias, C. Nieto-Granda, J. P. How, and L. Carlone, "Kimera-multi: Robust, distributed, dense metric-semantic slam for multi-robot systems," *IEEE Transactions on Robotics*, vol. 38, no. 4, 2022.
- [19] W. Luo and K. Sycara, "Minimum k-connectivity maintenance for robust multi-robot systems," in *2019 IEEE/RSJ International Conference on Intelligent Robots and Systems (IROS)*. IEEE, 2019, pp. 7370–7377.
- [20] W. Luo, S. Yi, and K. Sycara, "Behavior mixing with minimum global and subgroup connectivity maintenance for large-scale multi-robot systems," in *2020 IEEE International Conference on Robotics and Automation (ICRA)*. IEEE, 2020, pp. 9845–9851.
- [21] C. Lin, W. Luo, and K. Sycara, "Online connectivity-aware dynamic deployment for heterogeneous multi-robot systems," in *Proceedings of (ICRA) International Conference on Robotics and Automation*, May 2021.
- [22] G. Shi, W. Hönig, Y. Yue, and S.-J. Chung, "Neural-swarm: Decentralized close-proximity multirotor control using learned interactions," in *2020 IEEE International Conference on Robotics and Automation (ICRA)*. IEEE, 2020, pp. 3241–3247.
- [23] B. Rivière, W. Hönig, Y. Yue, and S.-J. Chung, "Glas: Global-to-local safe autonomy synthesis for multi-robot motion planning with end-to-end learning," *IEEE Robotics and Automation Letters*, vol. 5, no. 3, pp. 4249–4256, 2020.
- [24] M. Colledanchise, A. Marzinotto, D. V. Dimarogonas, and P. Ögren, "Adaptive fault tolerant execution of multi-robot missions using behavior trees," 2015. [Online]. Available: <https://arxiv.org/abs/1502.02960>
- [25] B. Şenbaşlar, W. Hönig, and N. Ayanian, "Rlss: real-time, decentralized, cooperative, networkless multi-robot trajectory planning using linear spatial separations," *Autonomous Robots*, vol. 47, no. 7, pp. 921–946, 2023.
- [26] R. K. Ramachandran, J. A. Preiss, and G. S. Sukhatme, "Resilience by reconfiguration: Exploiting heterogeneity in robot teams," in *2019 IEEE/RSJ International Conference on Intelligent Robots and Systems (IROS)*. IEEE, 2019, pp. 6518–6525.
- [27] A. Goeckner, X. Li, E. Wei, and Q. Zhu, "Attrition-aware adaptation for multi-agent patrolling," *arXiv preprint arXiv:2304.01386*, 2023.
- [28] W. Dai, H. Lu, J. Xiao, Z. Zeng, and Z. Zheng, "Multi-robot dynamic task allocation for exploration and destruction," *Journal of Intelligent & Robotic Systems*, vol. 98, pp. 455–479, 2020.
- [29] D. Krupke, M. Ernestus, M. Hemmer, and S. P. Fekete, "Distributed cohesive control for robot swarms: Maintaining good connectivity in the presence of exterior forces," in *2015 IEEE/RSJ International Conference on Intelligent Robots and Systems (IROS)*, 2015, pp. 413–420.
- [30] J. Hudack and J. Oh, "Multi-agent sensor data collection with attrition risk," in *Proceedings of the International Conference on Automated Planning and Scheduling*, vol. 26, 2016, pp. 166–174.
- [31] A. Halász, M. A. Hsieh, S. Berman, and V. Kumar, "Dynamic redistribution of a swarm of robots among multiple sites," in *2007 IEEE/RSJ international conference on intelligent robots and systems*. IEEE, 2007, pp. 2320–2325.
- [32] A. Prorok, M. A. Hsieh, and V. Kumar, "Formalizing the impact of diversity on performance in a heterogeneous swarm of robots," in *2016 IEEE International Conference on Robotics and Automation (ICRA)*. IEEE, 2016, pp. 5364–5371.
- [33] G. Notomista, S. Mayya, S. Hutchinson, and M. Egerstedt, "An optimal task allocation strategy for heterogeneous multi-robot systems," in *2019 18th European Control Conference (ECC)*. IEEE, 2019, pp. 2071–2076.
- [34] M. R. Pac, A. M. Erkmen, and I. Erkmen, "Control of robotic swarm behaviors based on smoothed particle hydrodynamics," in *2007 IEEE/RSJ International Conference on Intelligent Robots and Systems*. IEEE, 2007, pp. 4194–4200.
- [35] A.-R. Merheb, V. Gazi, and N. Sezer-Uzol, "Implementation studies of robot swarm navigation using potential functions and panel methods," *IEEE/ASME Transactions On Mechatronics*, vol. 21, no. 5, pp. 2556–2567, 2016.
- [36] F. Berlinger, M. Gauci, and R. Nagpal, "Implicit coordination for 3d underwater collective behaviors in a fish-inspired robot swarm," *Science Robotics*, vol. 6, no. 50, p. eabd8668, 2021.
- [37] L. C. Pimenta, G. A. Pereira, N. Michael, R. C. Mesquita, M. M. Bosque, L. Chaimowicz, and V. Kumar, "Swarm coordination based on smoothed particle hydrodynamics technique," *IEEE Transactions on Robotics*, vol. 29, no. 2, pp. 383–399, 2013.
- [38] L. Sabattini, N. Chopra, and C. Secchi, "Decentralized connectivity maintenance for cooperative control of mobile robotic systems," *The International Journal of Robotics Research*, vol. 32, no. 12, pp. 1411–1423, 2013.
- [39] N. Michael, M. M. Zavlanos, V. Kumar, and G. J. Pappas, "Maintaining connectivity in mobile robot networks," in *Experimental Robotics: The Eleventh International Symposium*. Springer, 2009, pp. 117–126.
- [40] M. Cardei and J. Wu, "Energy-efficient coverage problems in wireless ad-hoc sensor networks," *Computer communications*, vol. 29, no. 4, pp. 413–420, 2006.
- [41] S. Mini, S. K. Udgate, and S. L. Sabat, "M-connected coverage problem in wireless sensor networks," *International scholarly research notices*, vol. 2012, no. 1, p. 858021, 2012.
- [42] J. Scherer and B. Rinner, "Multi-robot persistent surveillance with connectivity constraints," *IEEE Access*, vol. 8, pp. 15 093–15 109, 2020.
- [43] Y. Wang, Y. Wang, Y. Cao, and G. Sartoretti, "Spatio-temporal attention network for persistent monitoring of multiple mobile targets," in *2023 IEEE/RSJ International Conference on Intelligent Robots and Systems (IROS)*. IEEE, 2023, pp. 3903–3910.
- [44] K. Su and F. Qian, "Multi-uav cooperative searching and tracking for moving targets based on multi-agent reinforcement learning," *Applied Sciences*, vol. 13, no. 21, p. 11905, 2023.
- [45] H. Kesten, "Percolation theory for mathematicians," *Progress in Probability and Statistics*, vol. 2, 1982.
- [46] I. Balberg, "Continuum percolation," *Encyclopedia of Complexity and Systems Science*, pp. 1443–1475, 2009.
- [47] S. Torquato, *Random heterogeneous materials: microstructure and macroscopic properties*. Springer Science & Business Media, 2002.
- [48] G. Grimmett, *Percolation*, 2nd ed. Springer-Verlag Berlin Heidelberg, 1999.
- [49] K. Zhang, Z. Yang, and T. Başar, "Multi-agent reinforcement learning: A selective overview of theories and algorithms," *Handbook of Reinforcement Learning and Control*, pp. 321–384, 2021.
- [50] J. Foerster, I. A. Assael, N. De Freitas, and S. Whiteson, "Learning to communicate with deep multi-agent reinforcement learning," *Advances in neural information processing systems*, vol. 29, 2016.
- [51] J. Chen and X. Ran, "Deep learning with edge computing: A review," *Proceedings of the IEEE*, vol. 107, no. 8, pp. 1655–1674, 2019.
- [52] S. He, S. Han, S. Su, S. Han, S. Zou, and F. Miao, "Robust multi-agent reinforcement learning with state uncertainty," *arXiv preprint arXiv:2307.16212*, 2023.
- [53] J. K. Gupta, M. Egorov, and M. Kochenderfer, "Cooperative multi-agent control using deep reinforcement learning," in *Autonomous Agents and Multiagent Systems: AAMAS 2017 Workshops, Best Papers, São Paulo, Brazil, May 8-12, 2017, Revised Selected Papers 16*. Springer, 2017, pp. 66–83.
- [54] S. Omidshafiei, J. Pazis, C. Amato, J. P. How, and J. Vian, "Deep decentralized multi-task multi-agent reinforcement learning under partial observability," in *International Conference on Machine Learning*. PMLR, 2017, pp. 2681–2690.
- [55] K. Nguyen, S. Schoedel, A. Alavilli, B. Plancher, and Z. Manchester, "Tinympc: Model-predictive control on resource-constrained microcontrollers," in *2024 IEEE International Conference on Robotics and Automation (ICRA)*. IEEE, 2024, pp. 1–7.
- [56] Y. Song, A. Romero, M. Müller, V. Koltun, and D. Scaramuzza, "Reaching the limit in autonomous racing: Optimal control versus reinforcement learning," *Science Robotics*, vol. 8, no. 82, p. eadg1462, 2023.